Quantitative evaluation of the pattern of shunt flow in the right ventricle and pulmonary artery of dogs with experimental ventricular septal defect.

M Nakai, … , T Togawa, K Ogino

J Clin Invest. 1983;72(3):779-788. https://doi.org/10.1172/JCI111049.

Research Article

Cineangiographic studies in patients with ventricular septal defect (VSD) have occasionally demonstrated that part of the blood across the defect is ejected immediately into the pulmonary artery (PA) passing through the outflow tract of the right ventricle (RV), but without being trapped in it. We attempted to make a quantitative evaluation of the flow of a partial shunt pathway (a direct VSD-PA pathway) that drains that part of the blood from the defect. Our method depended on a thermal dilution technique to obtain the ejection fraction of the RV and to observe a simultaneous pair of dilution curves at the roots of the aorta and PA after introduction of tracer into the left atrium. An analytical process was specially designed by incorporating a stable one-pass deconvolution technique. The method was applied to eight anesthetized dogs with acutely produced experimental VSD on the entrance of the outflow tract of the RV. The flow through the direct VSD-PA pathway was, in most cases, greater than 50 and up to 85% (mean of the eight, 57 +/- 5% SE) of the total left-to-right shunt flow. This would imply that less than 50%, and down to as little as 15%, of the total amount of shunt flow contributed to extra work of the RV in these cases. In addition, the impact on the pulmonary […]

Quantitative Evaluation of the Pattern of Shunt Flow in the Right Ventricle and Pulmonary Artery of Dogs with Experimental Ventricular Septal Defect

MASATSUGU NAKAI, TETSUO TOMINO, YOICHI GOTO, JIN YAMAMOTO, YUKIO MATSUI, TATSUO TOGAWA, and KOICHI OGINO, *Divisions of Cardiovascular Dynamics and Cardiovascular Surgery, National Cardiovascular Center, Suita, Osaka 565, Japan; Department of Medicine, Saga Medical University, Saga, Saga 840-01, Japan; Institute for Medical and Dental Engineering, Tokyo Medical and Dental University, Chiyodaku, Tokyo 101, Japan*

ABSTRACT Cineangiographic studies in patients with ventricular septal defect (VSD) have occasionally demonstrated that part of the blood across the defect is ejected immediately into the pulmonary artery (PA) passing through the outflow tract of the right ventricle (RV), but without being trapped in it. We attempted to make a quantitative evaluation of the flow of a partial shunt pathway (a direct VSD-PA pathway) that drains that part of the blood from the defect. Our method depended on a thermal dilution technique to obtain the ejection fraction of the RV and to observe a simultaneous pair of dilution curves at the roots of the aorta and PA after introduction of tracer into the left atrium. An analytical process was specially designed by incorporating a stable one-pass deconvolution technique. The method was applied to eight anesthetized dogs with acutely produced experimental VSD on the entrance of the outflow tract of the RV. The flow through the direct VSD-PA pathway was, in most cases, >50 and up to 85% (mean of the eight, 57±5% SE) of the total left-to-right shunt flow. This would imply that <50%, and down to as little as 15%, of the total amount of shunt flow contributed to extra work of the RV in these cases. In addition, the impact on the pulmonary vasculature due to such a large amount of pulsatile flow through the direct VSD-PA pathway may accelerate the development of hypertrophy of the pulmonary vessel wall.

Received for publication 30 August 1982 and in revised form 26 May 1983.

INTRODUCTION

In view of its pathophysiological importance, clinical investigators have studied the pattern of left-to-right shunt flow in patients with ventricular septal defect (VSD).[1] Levin et al. (1) first demonstrated in their cineangiographic study that part of the blood across the defect surges into the root of the pulmonary artery (PA) via the outflow tract of the right ventricle (RV) without being trapped in the RV. The remaining part of the blood across the VSD is directed toward the body of the RV, is trapped there, and eventually flows out of the RV into the PA during subsequent ventricular contractions. The partial shunt tract that drains blood across the VSD in the former manner is referred to in the text as a direct VSD-PA pathway, and in the latter manner, as a VSD-RV-PA pathway.

A method has yet to be established for the quantitative determination of partial shunt flows through these two pathways. The conventional oxygen saturation technique for such quantitative evaluation would require blood sampling from the RV, PA, and artery. The technique may thus not be entirely suitable, owing to poor mixing of the tracer, i.e., oxygen, with the blood in the RV. We designed an analytical process for this purpose by using a pair of thermal dilution curves sampled at the roots of the aorta and of the PA. In these vessels, the tracer may mix better

[1] *Abbreviations used in this paper:* LA, left atrium; LV, left ventricle; PA, pulmonary artery; RV, right ventricle; VSD, ventricular septal defect.

with the blood than in the RV. The principle of the process is analogous to that previously reported (2). In relation to the present study, we also discuss two well-known pathophysiological manifestations of the peculiar pattern of shunt flow in patients with VSD, i.e., the lesser degree of enlargement of the RV than of the left ventricle, and the progressive increase in flow resistance of the pulmonary circulation (3).

METHODS

Theoretical approach

We constructed our whole theory using a block flow model. During each heart cycle, blood and tracer were instantaneously transported toward the cardiovascular compartments, e.g., the cardiac ventricles and roots of the PA and aorta, and mixed there immediately. The tracer was assumed to be inert and nondiffusible, so that it was transported toward the PA and aorta from the site of tracer injection, without being lost outside the cardiovascular space. We further assumed that right-to-left shunt did not coexist, for the tracer returned to the left ventricle (LV) from the RV across the defect does not mix perfectly in the LV before being ejected into the aorta, RV, or PA (1).

Model for the left-to-right shunt pathway. We quantitatively described the flow pattern of the left-to-right shunt pathway by using a transport function (transfer or frequency function, transit time distribution, probability density function of transit time). The following discretized form of the function h can be introduced when it is considered to be a response at the root of the PA to a bolus placed at the orifice of the VSD during the heart cycle immediately before the first one:

$$h_i = \begin{cases} h_1 & (i = 1), \\ (1 - EF)^{i-2}\left(\dfrac{1}{\Delta t} - h_1\right)EF & (i \geq 2), \end{cases} \quad (1)$$

where i represents the serial number of the heart cycle; h_i, a value of h over the ith heart cycle; Δt, the time interval of a single heart cycle considered to be identical for all heart cycles; and EF, the ejection fraction of the RV.

This transport function is derived from a quantitative evaluation of the shape of a single-pass dilution curve that is free from the recirculating tracer (see Appendix). Briefly, this dilution curve would be obtained at the root of the PA after introduction of a bolus of tracer into the inflow of the VSD during the heart cycle immediately before the first (Fig. 1 *A*). The bolus becomes separated during the first heart cycle to enter into the direct VSD-PA pathway and VSD-RV-PA pathway (Fig. 1 *B*). The former part of the tracer yields the first value of the dilution curve at the PA (Fig. 1 *C*; Eq. 1, when $i = 1$). The latter part of the tracer is trapped in the RV during the first heart cycle (Fig. 1 *B*, *C*). It appears in parts in the PA during consecutive heart cycles, $i \geq 2$ (Fig. 1 *D*), to form a dilution curve that shows a geometric progression toward zero concentration (Eq. 1, when $i \geq 2$).

Fractional flows through the direct VSD-PA and VSD-RV-PA shunt pathways. We defined the mean flow expressed in blood volume per unit time through the PA as f_{lr}, that through the total left-to-right shunt as f_d, that through the direct VSD-PA pathway as f_{dp}, and that through the VSD-RV-PA pathway as f_{dr}. The fractional areas beneath

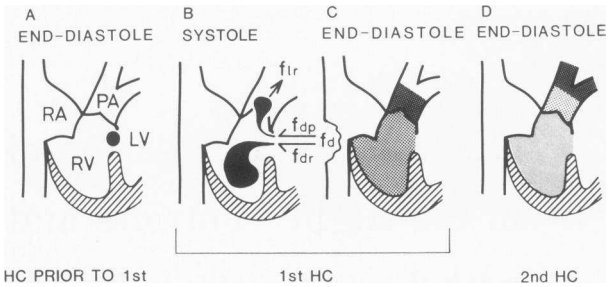

FIGURE 1. Schematic illustrations of the dual pathway of left-to-right shunt flow across the VSD. During the first ventricular ejection, the bolus of tracer, initially placed at the inflow of the VSD (*A*), becomes separated and surges into the root of the PA through the direct VSD-PA pathway, as well as into the body of the RV through the VSD-RV-PA pathway (*B*). The resultant concentrations at the PA and RV at ventricular end-diastole are illustrated by the shadings in *C*. Subsequent ventricular contraction ejects part of the latter component of the bolus into the PA, entirely eliminating the former component of the bolus from the root of the PA. Alternatively established concentrations at the PA and RV are illustrated by the shadings in *D*. *HC*, heart cycle; *RA*, right atrium.

the first ($i = 1$) and second ($i \geq 2$) components of the transport function represented by Eq. 1 correlate directly with the amounts of flows through these two partial shunt pathways (see Appendix):

$$\frac{f_{dp}}{f_d} = h_1 \Delta t, \quad (2)$$

and $f_{dr}/f_d = 1 - h_1\Delta t$, because $f_{dp} + f_{dr} = f_d$. To determine these two fractional flows is the final purpose of this study.

Relationship between h_i and a pair of tracer-dilution curves. Owing to technical difficulties, we cannot obtain h_i directly. We therefore designed a specific principle to extract h_i indirectly. This process uses the following relationship between h_i and a pair of dilution curves monitored at the roots of the aorta and PA, represented by I_i and O_i, respectively (see Appendix):

$$O_i = \sum_{j=1}^{i} \frac{f_d}{f_{lr}} I_j h_{i-j+1} \Delta t \quad (i = 1 \text{ to } it), \quad (3)$$

where it represents the serial number of a heart cycle during and before which recirculation of the tracer does not appear in the PA. During the first heart cycle, the tracer arrives at the root of the aorta, at the root of the PA through the direct VSD-PA pathway, and at the body of the RV through the VSD-RV-PA pathway. This relationship is a discrete approximation (4) of a convolution integral (5, 6). In practice, the pair of curves will be yielded by introduction of the tracer into the left atrium (LA).

The theory for the tracer-dilution technique requires complete mixing of the tracer at the in- and outflows (5). In our case, the tracer is required to mix well with blood within the LV (inflow) before it enters the direct VSD-PA and VSD-RV-PA pathways, and within the root of the PA (outflow) before it is sampled for determination of the dilution curve O_i. Moreover, the tracer is required to mix well within the root of the aorta before it is sampled for determination of the dilution curve I_i, which is a substitute for the dilution

curve at the inflow, i.e., LV (see below and Appendix). For this reason, the calculation needs to be carried out by using values for the dilution curves, I_t and O_t, at their full equilibrations to which, in practice, the curves attain only at end-diastole. Faster sample rates than one per single heart cycle would thus violate the requirement. Perfect mixing of the tracer in the RV is not an indispensable assumption, as long as the RV ejects the tracer at a uniform rate. The reason for selecting the root of the aorta, instead of the LV, as the sampling site is for obtaining a more stable dilution curve.

Deconvolution by multiple regression analysis. The process of calculating h_t from Eq. 3 is called numerical deconvolution. This process, however, tends to yield unreasonable oscillations and negative values in the results. To overcome this difficulty, we designed a deconvolution process with the aid of multiple regression analysis (7) in combination with simultaneous introduction of a fitting function for h_t. We have already performed the latter process by introducing Eq. 1 as the fitting function for h_t. The analysis yields the following working equations (see Appendix):

$$\frac{f_d}{f_{lr}} = \frac{\sum x_i^2 \sum y_i^2 - (\sum x_i y_i)^2}{\sum x_i z_i \sum y_i^2 - \sum x_i y_i \sum y_i z_i}, \quad (4)$$

$$\frac{f_{dp}}{f_d} = \frac{\sum x_i^2 \sum y_i z_i - \sum x_i y_i \sum x_i z_i}{\sum x_i^2 \sum y_i^2 - (\sum x_i y_i)^2} \Delta t, \quad (5)$$

where the sums are all carried out with respect to i, which runs from 1 to it. The values for x, y, and z are defined as follows:

$$x_i = \frac{O_i}{\Delta t} \qquad (i = 1 \text{ to } it), \quad (6)$$

$$y_i = \begin{cases} -I_1 & (i = 1), \\ EF \sum_{j=2}^{i} (1 - EF)^{j-2} I_{i-j+1} - I_i & (i = 2 \text{ to } it); \end{cases} \quad (7)$$

and

$$z_i = \begin{cases} 0 & (i = 1), \\ \frac{EF}{\Delta t} \sum_{j=2}^{i} (1 - EF)^{j-2} I_{i-j+1} & (i = 2 \text{ to } it). \end{cases} \quad (8)$$

EF can be obtained by monitoring the dilution curve at the PA yielded by a bolus injection of tracer into the RV (8).

Reconvoluted dilution curve at the PA. To evaluate the accuracy of the numerical computation of the deconvolution, a reconvolution was performed in each computational run by use of the calculated h_t. The process is to obtain the reconvoluted dilution curve at the PA, O'_i, according to the right side of Eq. 3. A comparison was made between the O'_i so calculated and experimentally obtained O_i dilution curves at the PA.

Predicted dilution curve in the RV. After the tracer injection into the LA, a dilution curve is also developed in the RV. To provide a straightforward confirmation of the validity of our principle, we will compare experimentally obtained, R_t, and analytically predicted, R'_t, dilution curves in the RV. The latter curve is obtained by a principle entirely identical to that for the derivations of Eqs. 3–5.

This dilution curve in the RV is calculated with the following equation by using preset values for the fractional flows, EF, Δt, and dilution curve at the aorta (see Appendix):

$$R'_i = \sum_{j=1}^{i} \frac{f_{dr}}{f_{lr} - f_{dp}} I_j r_{i-j+1} \Delta t \quad (i = 1 \text{ to } it - 1), \quad (9)$$

where

$$r_i = \frac{EF}{\Delta t} (1 - EF)^{i-1} \qquad (i = 1 \text{ to } \infty), \quad (10)$$

and r_t is the transport function of a partial shunt pathway from the VSD to the body of the RV (the partial VSD-RV pathway). The outflow of the partial VSD-RV pathway is assumed to be located in the body of the RV. The pathway is identical to the initial half of the VSD-RV-PA pathway. After the (it-1)th heart cycle, Eq. 9 no longer holds because of the recirculation of tracer appearing in the RV via the systemic circulation. Only for the introduction of Eqs. 9 and 10, is the tracer assumed to equilibrate well in the RV during each heart cycle.

We also predict a dilution curve at the RV that would be obtained when the direct VSD-PA pathway does not exist. This process is carried out by using Eqs. 9 and 10 with f_{dp} set at zero (see Appendix).

Experimental procedures

Surgical procedure. A total of eight mongrel dogs of both sexes, weighing 13±1 kg (mean±SE), were anesthetized with pentobarbital sodium (30 mg/kg i.v.; Abbott Laboratories, North Chicago, IL). The animals were artificially ventilated through a cuffed endotracheal tube with a mixture of oxygen and room air using a respirator (Mark 8, Bird Corp., Palm Springs, CA). Sufficient immobility of each animal was obtained with supplemental doses of pentobarbital (6–8 mg/kg i.v.), given when necessary. The femoral artery was cannulated for continuous recording of arterial blood pressure. The thoracic cage was opened widely by a sternal-splitting incision. The pericardium was sagittally incised. Its edges were attached to the thoracotomy margin to form a cradle for the heart. Heparin was introduced via a catheter inserted into the femoral vein (500 U/kg, Novo Research Institute, Bagsvaerd, Denmark). Experimental VSD was produced with a thin wall cylindrical boring tool 8 mm in diameter. The tool was introduced through the midpoint of a purse-string suture placed in the anterior wall of the RV.

We designed the experiment with cooled normal saline as the tracer. The time courses of the tracer concentration at the PA and aorta were monitored with thermistors. After producing the defect, we advanced a handmade catheter-tip thermistor into the root of the PA through the incision in the anterior wall of the RV. Another catheter-tip thermistor was placed at the root of the ascending aorta via an incision made in the apex of the LV. The catheters were then fixed firmly in position by tightening the suture.

Two cannulae for tracer-injection, both with blind tips and lateral openings, were advanced through one of the pulmonary veins and through the external jugular vein so that their tips were located in the LA and RV, respectively. The thorax was kept loosely open during the experiment. Intravenous low molecular weight dextran (Otsuka Pharmaceutical Co., Tokyo, Japan) in a volume of 50–100 ml was infused to combat hemorrhagic hypotension. At the end of each experiment, the animals were killed with an intravenous overdose of pentobarbital. Postmortem examinations were made of the location of the experimental VSD.

Observations of dilution curves for calculating fractional flows. Normal saline (0.5 ml) in a syringe was cooled to 10–15°C in an ice-water bath. Bolus introduction of the saline into the LA yielded a simultaneous pair of thermal dilution curves at the roots of the ascending aorta and of the PA, I_t and O_t, respectively. The circulatory system under analysis in our study consists of the cardiac ventricles and the roots

of the major vessels. The loss of the diffusible tracer, cooled saline, from the cardiovascular space may thus be as negligible as in the conventional thermodilution technique for the determination of cardiac output (8). Mixing of the tracer with the blood in the LV may be better with the tracer-injection into the LA than into the LV. The values for the dilution curves were sampled at each ventricular end-diastole, when the tracer equilibrates well in the roots of these two major vessels. Each end-diastolic point for sampling was identified by taking account of the simultaneously monitored time courses of right ventricular and arterial pressures.

A separate bolus of chilled saline introduced into the RV yielded a thermal dilution curve at the PA, permitting determination of *EF* for the RV. The simulataneous recordings of O_i and I_i were immediately preceded or followed by the separate determination of *EF* before the pattern of shunt flow underwent change.

In accord with our principle, it was necessary to sample values for O_i before the recirculating tracer contributed to it via the systemic circulation. To satisfy this requirement, we sampled values for the dilution curves usually over the first six, and at most over eight, heart cycles in a small number of cases.

Experimental and predicted dilution curves in the RV. In one animal, a comparison was made between the predicted and experimentally obtained dilution curves at the RV, R'_i, and R_i, respectively. For this purpose, three sets of dilution curves were monitored within a short period (Fig. 5): the dilution curve at the PA for determination of *EF*; a pair of dilution curves at the aorta I_i, and PA O_i (Fig. 5, left) for determination of the flow fractions f_{dp}/f_d and f_d/f_{tr}; and a pair of dilution curves at the aorta I_i and RV R_i (Fig. 5, right). To monitor the last set of dilution curves, the catheter-tip thermistor initially positioned in the PA was retracted until it rested within the body of the RV. For determination of the predicted dilution curves at the RV, the aortic dilution curve of the last set of curves was introduced into the right side of Eq. 9, together with the fractional flows and *EF* predetermined from the preceding two sets of dilution curves.

Instruments. The glass-bead thermistors used (Oízumí Manufacturing Co., Tokyo, Japan) were as small as 0.7 mm in diameter, allowing monitoring of rapid changes in temperature. They were mounted on plastic balls attached at the tips of Teflon catheters (1.2 mm in diameter) and protected by metal cages. The catheter-tip balls, 6 mm in diameter, were provided to improve mixing of the tracer at the roots of the PA and aorta. Signals from the thermistors were fed into Wheatstone bridges and amplifiers and displayed on a multichannel pen recorder (Biophysiograph, 140 System, San-ei Instruments Co., Tokyo, Japan). Calibration of the thermal dilution curves for absolute values of flow was not performed. However, we did calibrate the individual monitoring systems in vitro to assess the relative values for the simultaneous dilution curves, I_i and O_i or R_i, with respect to each other. The linearity of the systems covered a sufficiently wide range between the temperature at which the bridge was balanced and that at least 1.5°C below the balanced level. The data were processed on a computer (PDP 11/44, Digital Equipment Corp., Marlboro, MA).

Statistical analysis. In each animal, the data and results were averaged and expressed as the mean±SE. Comparisons were made for the χ^2 test of goodness of fit between the experimental dilution curve O_i and the reconvoluted curve O'_i (7). The influence of *EF* on the calculation of the fractional flows was examined by using two different values for *EF*, one observed and the other arbitrarily preset. The significance of the difference between these two results was evaluated by the paired t test (7). In both of the tests, the null hypothesis was considered to be acceptable when $P > 0.05$.

RESULTS

Location of the experimental VSD. All of the experimental VSD were found to be located adjacent to the right ventricular papillary muscle of the conus (Fig. 2). It was difficult to quantify the size of the defect because of the irregularly cut edges. The axial direction of the defect was always approximately perpendicular to the surface of the right ventricular septum.

Dilution curves. Fig. 3 shows typical records of the aortic and right ventricular pressures and a pair of dilution curves at the aorta and PA in dog 1. Note that the dilution curve at the PA develops simultaneously with that at the aorta during the first heart cycle. This was observed in every experimental run in all animals and definitely indicates that the direct VSD-PA pathway exists. Fig. 4 (bottom) illustrates a dilution curve at the PA for determination of *EF* as yielded by bolus injection of the tracer into the RV. The curve was obtained shortly after observation of the pair of dilution curves shown in Fig. 3. The aortic dilution curve did not develop before the sixth heart cycle, indicating absent right-to-left shunt across the VSD. This was the case in every animal.

Fractional shunt flows through the direct VSD-PA and VSD-RV-PA pathways. Two examples of results obtained from our deconvolution process are given in Fig. 3 (bottom) and Fig. 5 (left). The calculated transport functions h_i, drawn as solid straight lines, represent a large proportion of the fractional area during

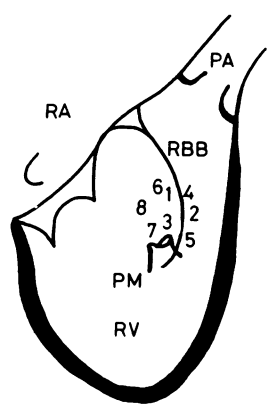

FIGURE 2 Locations of the experimental VSD, viewed from the right ventricular aspect. The numbers in the diagram are those of the animals and indicate the locations of the individual defects. *PM*, papillary muscle of the conus; *RBB*, right bundle branch; others as in legend to Fig. 1.

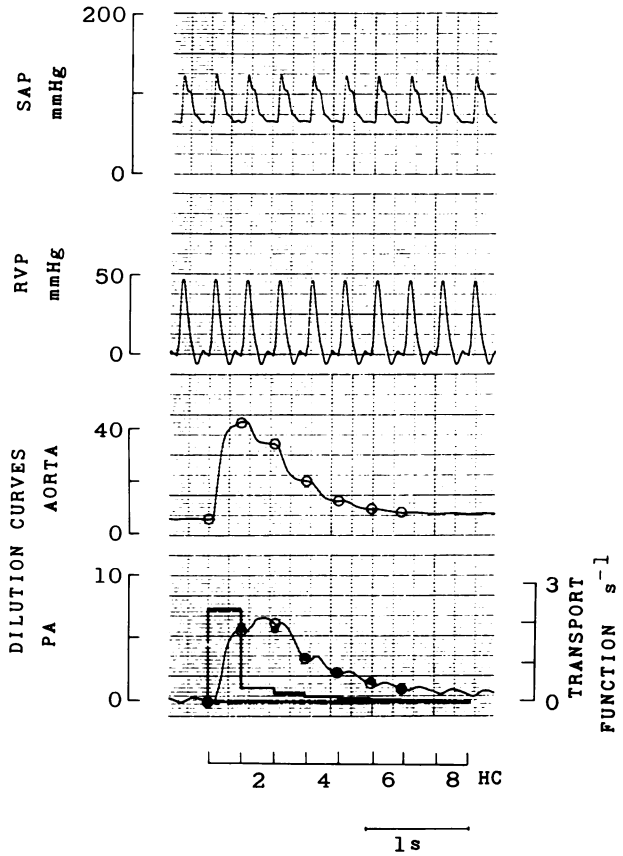

FIGURE 3 Typical set of records for systemic arterial pressure (*SAP*) and right ventricular pressure (*RVP*), and a pair of thermal dilution curves I_t and O_t at the aorta and *PA*, respectively, in dog 1. The scales for temperature are drawn arbitrarily but relative to each other. We sampled values of these dilution curves at each end-diastole during individual heart cycles. Points on the dilution curves selected for sampling are indicated by O. Our deconvolution technique extracted a trasport function of the shunt tract h_t (*bottom*, solid straight lines) with a large proportion of the fractional area (0.73) during the first heart cycle. The value of *EF* was 0.39. Reconvolution of the aortic dilution curve upon the transport function obtained, together with the calculated fractional flow through the total shunt (f_d/f_{lr} = 0.23), yielded a reconvoluted dilution curve at the PA O_t' (*bottom*, ●). A close resemblance is clearly seen between O_t' and O_t ($P > 0.5$, χ^2 test of goodness of fit).

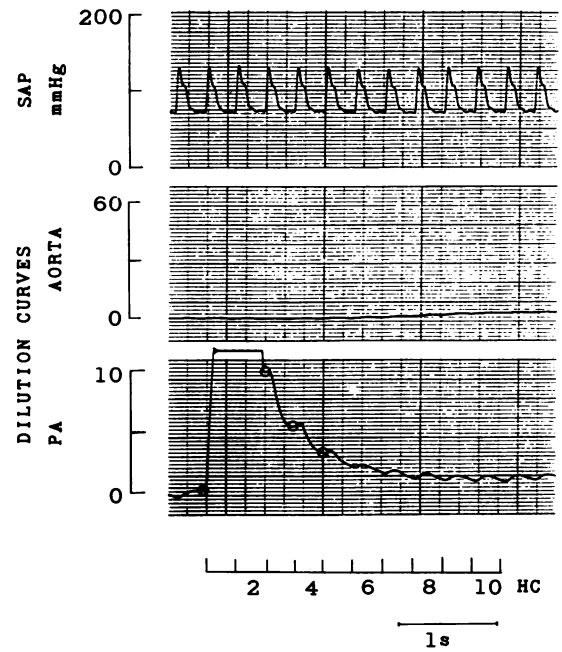

FIGURE 4 Records of thermal dilution curves at the aorta and PA yielded by bolus introduction of chilled saline into the RV for determination of *EF* of the RV. The dilution curve at the PA was saturated during the first heart cycle when mixing of the chilled saline with the blood in the RV might be incomplete. The value of *EF* was 0.39, as calculated by sampling values of the curve at the PA during three consecutive heart cycles. Points for sampling are indicated by O. Recirculation of the tracer was not apparent in the aortic dilution curve before the sixth heart cycle.

the first heart cycle. Table I summarizes the experimental data and calculated results. The values for *EF* of the RV were considerably low, ranging from 0.23 to 0.38 (mean±SE, 0.30±0.02). The ratio of the total shunt flow to the pulmonary arterial flow, f_d/f_{lr}, ranged between 0.16 and 0.72 (0.41±0.08).

The fractional shunt flow through the direct VSD-PA pathway f_{dp}/f_d was very large, ranging between 0.35 and 0.85 (0.57±0.05). In seven out of eight animals, the fractional flow was >0.50. In all cases, reconvolution to yield the calculated dilution curves at the PA O_t' resulted in an excellent similarity with the experimentally observed curves O_t ($P > 0.05$, χ^2 test of goodness of fit). Typical examples illustrating the good fit are given in Fig. 3 ($P > 0.5$, bottom) and Fig. 5 ($P > 0.9$, left).

Right ventricular dilution curve. Fig. 5 shows records of two sets of dilution curves yielded by two separate injections of the tracer into the LA, in dog 2; i.e., I_t and O_t (left), and I_t and R_t (right). Using these curves together with the predetermined *EF*, we calculated the two predicted dilution curves in the RV R_t' and compared these with the experimentally observed curve R_t (lower right).

First, we calculated the predicted curve assuming that the direct VSD-PA pathway does not exist. On the basis of this assumption, the value for f_d/f_{lr} was determined to be 0.24. The results for R_t' are indicated by solid triangles in the lower right panel. The finding that the experimentally observed curve R_t was much smaller than the calculated curve R_t' suggests that the

TABLE I
Summary of Results°

Dog	Body weight	n	Systemic arterial systolic pressure	Systemic arterial diastolic pressure	Right ventricular systolic pressure	Right ventricular diastolic pressure	*EF* (*n*)	f_d/f_{lr}	f_{dp}/f_d
	kg			*mmHg*					
1	12	7	123±1	64±1	51±1	1±1	0.38±0.02 (5)	0.23±0.01	0.67±0.02
2	12	6	153±2	100±2	45±1	8±1	0.34±0.01 (5)	0.20±0.01	0.50±0.03
3	12	4	132±2	59±1	44±1	13±1	0.26±0.01 (4)	0.50±0.01	0.85±0.03
4	15	3	152±1	102±1	42±2	6±1	0.25±0.02 (3)	0.64±0.03	0.53±0.05
5	13	6	123±1	98±1	44±1	6±1	0.26±0.01 (3)	0.16±0.01	0.35±0.03
6	15	2	118±2	66±2	28±0	6±1	0.32 (1)	0.50±0.01	0.51±0.03
7	14	2	122±2	75±0	35±1	5±0	0.38 (1)	0.29±0.01	0.59±0.02
8	10	1	140	90	34	3	0.23 (1)	0.72	0.58
Mean of 8 animals			133±5	82±6	40±3	6±1	0.30±0.02	0.41±0.08	0.57±0.05

° Mean±SE.

assumption of an absent VSD-PA pathway is not realistic.

We next calculated the predicted dilution curve R'_t, assuming that the direct VSD-PA pathway does exist. Based on this assumption, the value for f_d/f_{lr} was determined to be 0.26. In spite of the different processes for calculating f_d/f_{lr}, i.e., one was with and the other without assuming the direct VSD-PA pathway, the values were virtually identical. The results for R'_t are plotted as solid circles (lower right). Although

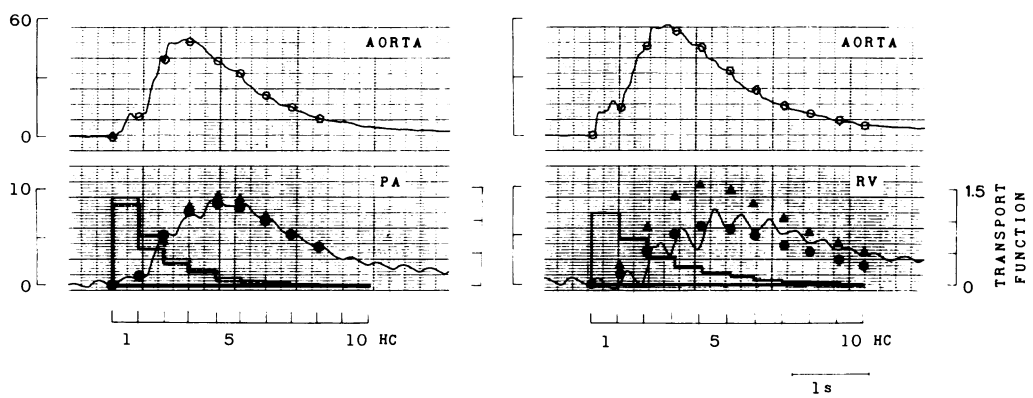

FIGURE 5 Two sets of dilution curves (transport function in seconds^{-1}) monitored at the aorta I_t and PA O_t (*left*) and at the aorta I_t and RV R_t (*right*). Points for sampling values of curves at the aorta are indicated by O. We did not indicate the points for sampling the curves at the PA for keeping clarity of the illustration (*lower left*), and at the RV because of difficult sampling owing to rapid and irregular oscillations of the curve (*lower right*). The ejection fraction of the RV was previously determined (0.38) for calculating the transport function of the partial VSD-RV pathway r_t (*lower right*, indicated by straight lines). The aortic curve I_t of the latter set of curves (*upper right*) and r_t were used for calculation of the predicted dilution curves at the RV R'_t on the assumption that the direct VSD-PA pathway does not exist (▲) or that it does exist (●, *lower right*). Under the latter assumption, the process predicted the experimental curve R_t better than that carried out under the former assumption. The flow fraction f_d/f_{lr} (0.24) was obtained by using the pair of dilution curves I_t and O_t (*left*) in the calculation on the former assumption that the direct VSD-PA pathway does not exist. The process extracted a transport function (*lower left*, broken lines). On the latter assumption that the direct pathway exists, the flow fractions f_d/f_{lr} (0.26) and f_{dp}/f_d (0.48) were obtained by utilizing the same pair of dilution curves (*left*). The process extracted another transport function (*lower left*, straight lines), which was similar to that calculated with the former assumption. Reconvolutions of I_t with the transport functions so obtained yielded similar dilution curves at the PA O'_t to the experimental curve O_t, both in the calculation without (▲, $P > 0.9$, χ^2 test of goodness of fit) and in that with the assumption of the direct VSD-PA pathway (●, $P > 0.9$).

large oscillations of R_i rendered a quantitative comparison impossible, the calculated values for R'_i correlated well with the individual peaks of the oscillations of R_i up to the fourth heart cycles. In the descending limb, the experimental right ventricular curve was slightly larger than the predicted one. This discrepancy may indicate arrival of the recirculating tracer at the RV through the systemic circulation. Overall, we conclude that there was a good resemblance between the predicted dilution curve in the RV calculated on the assumption of a coexisting direct VSD-PA pathway, and the experimental right ventricular dilution curve.

DISCUSSION

Assessment of the methodology

Validity of our model for the intracardiac flow pattern of left-to-right shunt. Our principle for data analysis depends on deconvolution from a discretized form of the convolution integral for obtaining a transport function from a pair of in- and outflow tracer dilution curves (4–6). The deconvolution process is, however, generally highly sensitive to experimental errors imposed on the pair of dilution curves (2, 4, 9–12). Bassingthwaighte (13) assumed a single fitting function with several parameters as a mathematical model for the entire time course of the transport function. An iterative adjustment of the parameters affects stable deconvolution to select the most reasonable transport function by questioning at each time whether or not the convolution equation is sufficiently approximated.

To verify the fitting function as a reasonable model for the pattern of flow, it is necessary for its introduction to provide a theoretical or empirical reason (12). In our case, we obtained experimental data to show that the dilution curve at the PA O_i developed during the first heart cycle simultaneously to that at the aorta I_i (Figs. 3 and 5), and that the size of the experimentally observed curve at the RV R_i was much smaller than the predicted curve R'_i, which should be the case if the left-to-right shunt was devoid of the direct VSD-PA pathway (Fig. 5). These two findings clearly indicate that the VSD-RV-PA pathway coexists with the direct VSD-PA pathway and that a considerable amount of blood is transported through the latter pathway.

The intravascular volume of the root of the PA is sufficiently small relative to the flow through it. It seems realistic, therefore, to assume, as we did in our basic principle (see Appendix for derivation of Eq. 1), that the tracer that has been transported through the direct VSD-PA pathway into the root during any one of the heart cycles is totally washed out during the next cycle. The tracer trapped in the RV during any one of the heart cycles is postulated to be ejected in parts during subsequent cycles and to yield a dilution curve at the PA whose descending limb shows a geometric progression. This assumption is also reasonable, as experimentally proven in Fig. 4, and is widely accepted in the theory for determination of the ventricular ejection fraction (8). Our fitting function Eq. 1 representing the model for the intracardiac pattern of left-to-right shunt flow thus satisfies the requirement for empirical as well as theoretical reasons.

In addition, when the direct VSD-PA pathway was assumed to exist, the reconvolution resulted in an equivalent size of predicted dilution curve at the RV R'_i to the experimentally obtained curve R_i. When the direct VSD-PA pathway was assumed to be absent, the reconvolution resulted in a much larger predicted curve than the experimental one (Fig. 5). These findings provide a straightforward confirmation of the validity of our principle for determination of the fractional flow f_{dp}/f_d through the direct VSD-PA pathway.

We obtained good similarities between the reconvoluted and experimentally obtained dilution curves at the PA (Figs. 3 and 5). Although such close resemblances are not a test of the uniqueness of our fitting function, while necessary (10), they do support the accuracy of the computation of the deconvolution processes.

Deconvolution with multiple regression analysis. As early as 1952, Paynter (4) suggested the advantages of deconvolution performed in combination with simultaneous introduction of multiple linear regression analysis. His idea is very sensible, since such statistical computation does not pay too much attention to erroneous experimental values appearing in the tracer-dilution curves. This favorable feature apparently holds true in our case, in which the fractional flows were calculated by carrying out the deconvolution, taking account of all the sampled values of dilution curves (Eqs. 4–8). Additionally, the process suggested by Paynter (4) allows one-pass computation without iteration. It was shown that with this treatment the inherent instability of the deconvolution was much improved but still persisted (2). For this reason, Nakai (2) attempted deconvolution and regression analysis in additional combination with a technique assuming weighted simple fitting functions for every small segment of the transport function.

This process requires iteration but extracts a reasonable transport function. In the present study also, the method was shown to be a powerful technique for carrying out stable deconvolution when introducing simultaneously not only the multiple regression analysis but also the fitting function for the transport func-

tion. Such was indeed the case also in the method proposed by Knopp et al. (14), who adopted prechosen multiple fitting functions for the transport function.

Present experimental model in relation to human VSD

The pathophysiological state of our experimental animals may be designated as falling into the group with medium-sized defect with normal pulmonary vascular resistance and moderately elevated right ventricular pressure. The defect in the ventricular septum was placed on the entrance of the outflow tract of the RV. All the animals used in the present study developed a substantial amount of flow through the direct VSD-PA pathway. In patients with VSD, however, such frequent incidence has not been found to hold true, as experienced in our cineangiographic examinations of the intracardiac pattern of shunt flow. We would regard our experimental VSD as functionally the same as some subtype of human defect in which the direct VSD-PA pathway coexists.

The right ventricular *EF* was considerably lower in the present study than that (mean, 0.62) reported in patients with VSD (15). The purse-suture placed in the anterior wall of the RV would be responsible for a reduction in right ventricular performance together with acute right ventricular volume overload due to left-to-right shunt. The value for *EF*, however, cannot be considered a significant variable that critically influences the values of the fractional flows f_d/f_{lr} and f_{dp}/f_d. This inference is derived from the finding that f_{dp}/f_d, which is independent of *EF*, is great; and the fact that the sole determinant of f_d/f_{lr} is the size of the dilution curve at the PA, not the time course of the curve.

To confirm the small influence of *EF* on the results, we calculated the fractional flows under an *EF* value preset at 0.62 (Table II and reference 15). Differences in values for f_{dp}/f_d between that calculated with the observed *EF* and that with the preset *EF* were often statistically significant, but quite small in all animals except one. The larger difference in dog 5 was due to a smaller proportion of the fractional flow f_{dp}/f_d (0.35±0.03). The influence of these two different values for *EF* on f_d/f_{lr} is also trivial. In this calculation with arbitrarily present values of *EF*, the reconvoluted curves O_i' were similar to the experimental curves O_i ($P > 0.05$, χ^2 test of goodness of fit).

Implications of the present study

The most striking result obtained in the present study was that the partial shunt flow through the direct VSD-PA pathway was great. The amount ranged between 35 and 85% of the total shunt flow. The amount was >50% in seven cases out of eight. In other words, in most cases <50%, and down to as little as 15%, of the total shunt flow entered the RV through the VSD-RV-PA pathway. Only this small component of shunt flow contributed to extra work of the RV.

Levin et al. (1) were the first to demonstrate the direct VSD-PA component of the shunt tract in their cineangiographic study. Its pathophysiological significance concerns one of the well known manifestations of patients with VSD, i.e., the lesser degree of enlargement of the RV than of the LV before pulmonary hypertension develops. This point was argued by Graham et al. (3) in their suggestive review. As they say, "since normally the major shunting occurs during ventricular systole and is ejected into the outflow tract of the right ventricle, the right ventricle does not enlarge to the same extent as the left ventricle." Their analysis is in accord with our quantitative finding that the fractional flow through the VSD-RV-PA pathway f_{dr}/f_d is very small.

Another characteristic feature of patients with VSD is the progressive increase in pulmonary vascular resistance with medial hypertrophy and intimal proliferation (16). The basic mechanisms giving rise to such

TABLE II
Effects of EF on the Fractional Shunt Flows

Dog	n	EF (n)	f_d/f_w	f_{dp}/f_d
1	7	0.38±0.02 (5)	0.23±0.01	0.67±0.02
		0.62	0.22±0.01*	0.68±0.02*
2	6	0.34±0.01 (5)	0.20±0.01	0.50±0.03
		0.62	0.18±0.01*	0.47±0.04
3	4	0.26±0.01 (4)	0.50±0.01	0.85±0.03
		0.62	0.47±0.01*	0.88±0.04*
4	3	0.25±0.02 (3)	0.64±0.03	0.53±0.05
		0.62	0.54±0.04	0.53±0.08
5	6	0.26±0.01 (3)	0.16±0.01	0.35±0.03
		0.62	0.12±0.01*	0.28±0.06
6	2	0.32 (1)	0.50±0.01	0.51±0.03
		0.62	0.44±0.02	0.49±0.05
7	2	0.38 (1)	0.29±0.01	0.59±0.02
		0.62	0.26±0.02	0.59±0.01
8	1	0.23 (1)	0.72	0.58
		0.62	0.60	0.66

Data from dogs 4, 6, 7, and 8 were not evaluated statistically because of the small number of measurements.
* Statistically significant differences between the results ($P < 0.05$, paired t test).

manifestations remain to be clarified (3). However, increased stress on the pulmonary vessel wall driven by "a common ejectile force from both ventricles" (3) may directly or indirectly trigger such changes (3, 17). The impact of flow conducted through the direct VSD-PA pathway should be especially marked in the pulmonary vessels, because a high flow velocity across the VSD is not damped by the RV. Thus, when the flow through the direct VSD-PA pathway is great in proportion to the total pulmonary flow, i.e., f_{dp}/f_{lr}, the mechanisms leading to pathological changes of the pulmonary vessel wall may operate more efficiently.

APPENDIX

Glossary

i or j	serial number of the heart cycle
it	serial number of the heart cycle during and before which the dilution curve at the PA is free from recirculating tracer
Δt	time interval of a single heart cycle considered to be equal for all heart cycles
C_i	value of a single-pass dilution curve obtained during the ith heart cycle at the root of the PA in response to a bolus tracer injection
I_i	tracer-dilution curve recorded at the root of the aorta
O_i	dilution curve at the root of the PA
O'_i	reconvoluted dilution curve at the PA
R_i	dilution curve in the RV
R'_i	predicted dilution curve in the RV
h_i	transport function of the total shunt pathway from the VSD to the PA
r_i	transport function of the partial VSD-RV pathway
f_{lr}	mean total blood flow through the PA expressed as blood volume/unit time
f_d	mean total left-to-right flow across the VSD
f_{dp}	mean flow through the direct VSD-PA pathway
f_{dr}	mean flow through the VSD-RV-PA pathway
EF	ejection fraction of the RV
Q	total amount of tracer-bolus introduced during a single heart cycle into the inflow of the VSD
α, β	estimates of f_{lr}/f_d and $f_{dp}/f_d\Delta t$, respectively
x_i, y_i, z_i	variables of a set of simultaneous equations
e_i	discrepancy between z and the value determined from α, β, x, and y caused by experimental error

Derivation of Eq. 1. The single-pass dilution curve, denoted here by C_i, during the first heart cycle, C_1, consists solely of the tracer drained from the direct VSD-PA pathway (Fig. 1 *C*). Subsequent ventricular ejection during the second heart cycle will totally eliminate this part of the tracer from the root of the PA (Fig. 1 *D*). The dilution curve at the PA after the first heart cycle consists of the tracer drained from the VSD-RV-PA pathway. The time course of the curve will show a geometric progression towards zero concentration. The ratio C_i/C_{i-1} will thus be equivalent to $1\text{-}EF$ (8).

The entire time course of C_i is expressed as

$$C_i = \begin{cases} C_1 & (i = 1), \\ (1 - EF)^{i-2} C_2 & (i \geq 2). \end{cases} \tag{11}$$

To standardize C_i for convenience in further discussions, we introduce a discretized form of the transport function h defined as

$$h_i = \frac{C_i}{\sum_{j=1}^{\infty} C_j \Delta t} \quad (i = 1 \text{ to } \infty). \tag{12}$$

We obtain Eq. 1 from Eq. 11 by the use of this relationship and by taking into account the solution that $\Sigma(1 - EF)^{i-2}$ converges to $1/EF$ as i proceeds from 2 up to infinity, and the area beneath the entire time course of the function is unity: $\Sigma h_j \Delta t = 1$, where j runs from 1 up to infinity.

Derivation of Eq. 2. We introduce Eq. 2 by utilizing the single-pass dilution curve C_i. Let Q represent the total amount of tracer appearing in the PA through the left-to-right shunt pathway. We then obtain $Q = \Sigma f_{lr} \Delta t C_j$, where j takes values from 1 up to infinity. This relationship becomes $Q = f_{lr} C_1 / h_1$ by considering Eq. 12 when $i = 1$. Since the amount of tracer entering the direct VSD-PA pathway, $(f_{dp}/f_d)Q$, is identical to that appearing in the PA during the first heart cycle, $f_{lr} \Delta t C_1$, we obtain Eq. 2.

Derivation of Eq. 3. The mathematical analysis is basically the same as that described by Zierler (5) when quantitatively evaluating a component of recirculation superimposed on a single-pass dilution curve of tracer. The dilution curve at the aorta I_i is considered to consist of a train of square waves of concentration $I_1, I_2, \ldots I_{it}$, which develop during the individual heart cycles over a period of Δt. The individual square wave at the aorta during, say, the jth heart cycle, also represents that in the LV during the immediately preceding cycle $j - 1$. The configuration of the single-pass dilution curve at the PA, which would be obtained in response to only this square wave in the LV, should be essentially identical to that of h_i. However, as in Zierler's (5) analysis, the magnitude of its concentration and the location on the time axis depend on those of the square wave in the LV. The dilution curve at the PA O_i should consist of all such individual single-pass curves. The flow ratio f_d/f_{lr} is introduced in Eq. 3, since the dilution curve I enters the shunt pathway with a flow f_d, whereas the curve O is carried by the pulmonary arterial flow at an amount of f_{lr}.

Derivation of Eqs. 4 and 5. First, we must rearrange Eq. 3 to facilitate our purpose of applying linear regression analysis. Rearrangement with respect to the two unknown coefficients, f_d/f_{lr} and h_1, together with substitution of the right side of Eq. 1 for h_i that appears in Eq. 3, yields the following it simultaneous equations:

$$\frac{f_{lr}}{f_d} \cdot \frac{O_1}{\Delta t} - h_1 I_1 = 0 \quad (i = 1),$$

$$\frac{f_{lr}}{f_d} \cdot \frac{O_i}{\Delta t} + h_1 \left[EF \sum_{j=2}^{i} (1 - EF)^{j-2} I_{i-j+1} - I_i \right] = \frac{EF}{\Delta t} \sum_{j=2}^{i} (1 - EF)^{j-2} I_{i-j+1} \quad (i = 2 \text{ to } it). \tag{13}$$

These equations are linear with respect to the coefficients f_{lr}/f_d and h_1 when EF, I_i, Δt, and O_i are known.

Eq. 13 describes a precise relationship. In practice, however, we cannot draw the relationship accurately, because observational errors are inevitably involved in the experimentally obtained values for the dilution curves, EF, and Δt. For simplicity, let x, y, and z be the values determined by such experimental measurements (Eqs. 6–8) and correspond to the variables of the simultaneous equations ex-

pressed by Eq. 13. We then introduce the following relationship which simulates Eq. 13:

$$\alpha x_i + \beta y_i = z_i + e_i \quad (i = 1 \text{ to } it), \tag{14}$$

where α and β are to be obtained from x, y, and z to estimate f_{lr}/f_d and h_l, respectively; and e_i represents an unavoidable discrepancy caused by experimental error between the left side of Eq. 14 and z_i.

The regression analysis (7) approximates Eq. 14 to the precise relationship Eq. 13 in such a way that the sum of the squared e_i is minimal by adjusting α and β. The values for α and β so obtained will satisfy, albeit not perfectly, all of the relationships between x, y, and z. By substituting f_{lr}/f_d and $f_{dp}/f_d\Delta t$ for α and β, respectively, the analysis finally yields Eqs. 4 and 5.

Derivation of Eqs. 9 and 10. The following consideration gives rise to Eq. 10: A single-pass dilution curve in the RV responding to a bolus injection of tracer into the orifice of the VSD reduces its concentration in a geometric progression. The theoretical approach for Eq. 9 is identical to that for Eq. 3, except in the following respects: The dilution curve in the RV consists of the tracer trapped in the RV in the passage through the VSD-RV-PA pathway to the PA, the flow through the pathway is f_{dr}, and the amount of flow that dilutes the tracer in the RV is $f_{lr} - f_{dp}$.

Derivation of the predicted dilution curve at the RV when the direct VSD-PA pathway does not exist. In this case, f_{dp} is set at zero and therefore $f_{dr} = f_d$ for Eq. 9. Since we assume arbitrarily in this case that the direct VSD-PA pathway does not exist, the value for f_d/f_{lr} has to be calculated in a manner different from that using Eq. 4. The alternative process is the same as that reported previously (2). Briefly, we deconvolute Eq. 3 for extracting a curve of $(f_d/f_{lr})h_i$ from I_i and O_i with simultaneous introduction of multiple regression analysis and a few restrictions. The restrictions adopted are as follows: Each small segment on the curve follows a quadratic curve, and the value for $(f_d/f_{lr})h_i$ is zero after the eighth heart cycle. The former restriction is used for smoothing of the curve, never as an assumption for the intracardiac flow pattern of the shunt. The fractional flow f_d/f_{lr} is identical to the area beneath the $(f_d/f_{lr})h_i$ curve so obtained.

REFERENCES

1. Levin, A. R., M. S. Spach, R. V. Canent, Jr., J. P. Boineau, M. P. Capp, V. Jain, and R. C. Barr. 1967. Intracardiac pressure-flow dynamics in isolated ventricular septal defects. *Circulation.* 35:430–441.
2. Nakai, M. 1981. Computation of transport function using multiple regression analysis. *Am. J. Physiol.* 240(Heart Circ. Physiol. 9):H133–H144.
3. Graham, T. P., Jr., H. W. Bender, and M. S. Spach. 1977. Defects of the ventricular septum. *In* Heart Disease in Infants, Children, and Adolescents. A. J. Moss, F. H. Adams, and G. C. Emmanouillides, editors. Williams & Wilkins Co., Baltimore. Second ed. 140–161.
4. Paynter, H. M. 1952. Methods and results from M.I.T. studies in unsteady flow. *Boston Soc. Civil Eng. J.* 39:120–165.
5. Zierler, K. L. 1962. Theoretical basis of indicator-dilution methods for measuring flow and volume. *Circ. Res.* 10:393–407.
6. Stephenson, J. L. 1948. Theory of the measurement of blood flow by the dilution of an indicator. *Bull. Math. Biophys.* 10:117–121.
7. Miller, I., and J. E. Freund. 1977. Probability and Statistics for Engineers. Prentice-Hall Inc., Englewood Cliffs, New Jersey. Second ed.
8. Yang, S. S., L. G. Bentivoglio, V. Maranhao, and H. Goldberg. 1978. From Cardiac Catheterization Data to Hemodynamic Parameters. F. A. Davis Co., Philadelphia. Second ed. 101–151.
9. Coulam, C. M., H. R. Warner, E. H. Wood, and J. B. Bassingthwaighte. 1966. A transfer function analysis of coronary and renal circulation calculated from upstream and downstream indicator-dilution curves. *Circ. Res.* 19:879–890.
10. Gamel, J., W. F. Rousseau, C. R. Katholi, and E. Mesel. 1973. Pitfalls in digital computation of the impulse response of vascular beds from indicator-dilution curves. *Circ. Res.* 32:516–523.
11. Maseri, A., P. Caldini, S. Permutt, and K. L. Zierler. 1970. Frequency function of transit times through dog pulmonary circulation. *Circ. Res.* 26:527–543.
12. Neufeld, G. R. 1971. Computation of transit time distributions using sampled data Laplace transforms. *J. Appl. Physiol.* 31:148–153.
13. Bassingthwaighte, J. B. 1966. Plasma indicator dispersion in arteries of the human leg. *Circ. Res.* 19:332–346.
14. Knopp, T. J., W. A. Dobbs, J. F. Greenleaf, and J. B. Bassingthwaighte. 1976. Transcoronary intravascular transport functions obtained via a stable deconvolution technique. *Ann. Biomed. Eng.* 4:44–59.
15. Graham, T. P., Jr., G. F. Atwood, R. J. Boucek, Jr., D. Cordell, and R. C. Boerth. 1976. Right ventricular volume characteristics in ventricular septal defect. *Circulation.* 54:800–804.
16. Dammann, J. F., Jr., W. M. Thompson, Jr., O. Sosa, and I. Christlieb. 1960. Anatomy, physiology and natural history of simple ventricular septal defects. *Am. J. Cardiol.* 5:136–166.
17. Wood, P. 1968. Diseases of the Heart and Circulation. Eyre & Spottiswoode, London. Third ed. 964–985.